PHYSICAL REVIEW MATERIALS **5**, 074801 (2021)

Superconductivity and magnetism in $R_4Be_{33}Pt_{16}$ (R = Y, La–Nd, Sm–Lu): A family of crystallographically complex noncentrosymmetric compounds

E. Svanidze,[1] A. Amon,[1] M. Nicklas,[1] Yu. Prots,[1] M. Juckel,[1] H. Rosner,[1] U. Burkhardt,[1] M. Avdeev,[2] Yu. Grin,[1] and A. Leithe-Jasper[1]

[1]*Max-Planck-Institut für Chemische Physik fester Stoffe, Nöthnitzer Straße 40, Dresden 01187, Germany*
[2]*Australian Nuclear Science and Technology Organisation, Lucas Heights, New South Wales 2234, Australia*

(Received 12 April 2021; revised 31 May 2021; accepted 21 June 2021; published 14 July 2021)

Crystallographically complex compounds often possess peculiar physical properties, the evolution of which can be tracked by changing one of the constituent elements at a time. We report the discovery and synthesis of isotypic $R_4Be_{33}Pt_{16}$ (R = Y, La–Nd, Sm–Lu) compounds, which crystallize with the noncentrosymmetric cubic space group $I\bar{4}3d$. The lattice parameters vary from $a = 13.6682(4)$ Å for R = La to $a = 13.4366(3)$ Å for R = Lu. $R_4Be_{33}Pt_{16}$ phases exhibit a wide range of ground states. R = Y, La, and Lu analogs display superconductivity. Their calculated electronic structures show nonzero density of states at the Fermi level, with the value of the Sommerfeld coefficient consistent with those obtained experimentally. The rest of the $R_4Be_{33}Pt_{16}$ compounds exhibit magnetic ground states with ordering temperatures ranging from $T_{\mathrm{mag}} = 0.4$ K (R = Yb) to $T_{\mathrm{mag}} = 40$ K (R = Pr). The diversity of physical properties of $R_4Be_{33}Pt_{16}$ compounds can likely be attributed to the nature of the individual rare-earth elements, structural noncentrosymmetry, the large number of atoms per unit cell (212), as well as the complex multicenter interactions within the Be-Pt framework.

DOI: 10.1103/PhysRevMaterials.5.074801

I. INTRODUCTION

Complex crystal structures often yield fascinating physical properties [1–12], which makes the search for new materials of acute interest to the condensed matter physics and solid-state chemistry communities. In particular, the variation of one constituent element in a series of isostructural compounds can be used to pinpoint the trends that govern the relation between the crystal structure and the resultant physical properties, pushing us one step closer to being able to create the much-needed materials by design. Among rare-earth-based intermetallic compounds, the diverse span of properties is mostly driven by the interplay of the $4f$ orbitals with the conduction s, p, or d electrons, which, in turn, can be tuned by the spatial separation and concentration of the rare-earth ions. With this in mind, several families of rare-earth-based materials have been previously studied [13–24].

The initial interest in rare-earth- and platinum-based materials was spiked by the discovery of the noncentrosymmetric superconductor $CePt_3Si$ ($T_c = 0.75$ K) [25]. Further studies reported a series of borocarbides RPt_2B_2C (R = rare-earth element), which from the point of view of their crystal structure can be related to the 122-type high-temperature superconductors. It was established that some of these materials also superconduct, but at much lower critical temperatures ($T_c^{\mathrm{max}} \approx 11$ K for YPt_2B_2C [26]). Another member of the family, $NdPt_2B_2C$, exhibits coexistence of superconductivity and magnetism [27]. On the other hand, the number of known rare-earth and beryllium-based compounds is somewhat limited, with the only reported series being the RCu_4Be family [28]. None of the RCu_4Be compounds show superconductivity.

In this exploratory work, we present physical properties of 15 isostructural compounds $R_4Be_{33}Pt_{16}$ (R = Y, La–Nd, Sm–Lu). They are representatives of a new structure type, possessing a cagelike crystal structure, similar to clathrates. The crystal structure was established and described in detail for $Y_4Be_{33}Pt_{16}$ in our previous publication [29] and for $La_4Be_{33}Pt_{16}$ in the current work (see Sec. SI of the Supplemental Material [30]). In contrast to the mostly two-center bonding in the framework of clathrate compounds, the new $R_4Be_{33}Pt_{16}$ materials reveal the multicenter interactions within the framework, caused by the demand of the valence electrons in the system [29].

The physical properties of the $R_4Be_{33}Pt_{16}$ phases are quite diverse. For R = Y, La, and Lu, superconductivity was observed below $T_c = 0.9$, 2.5, and 0.7 K, respectively. Their electronic structure was investigated by means of density functional theory calculations. The rest of the $R_4Be_{33}Pt_{16}$ compounds exhibit magnetic ground states. All of $R_4Be_{33}Pt_{16}$ compounds display modest values of the electronic specific coefficient γ_n.

II. EXPERIMENTAL METHODS

The sample preparation was performed in a specialized laboratory, equipped with an argon-filled glove box system (MBraun, $p(H_2O/O_2) < 0.1$ ppm) [31]. Polycrystalline

---

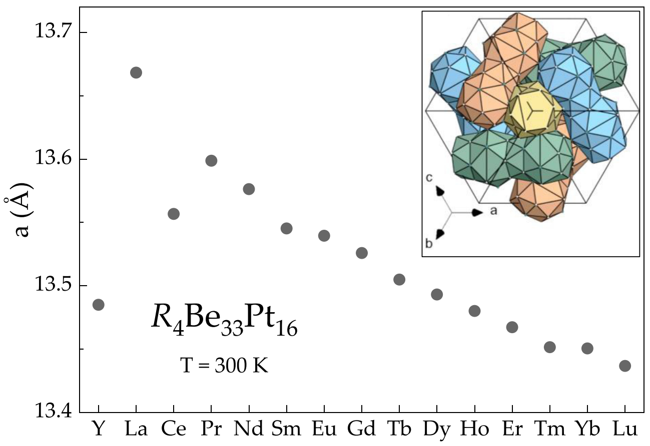

FIG. 1. The cubic lattice parameter a for the $R_4Be_{33}Pt_{16}$ (R = Y, La–Nd, Sm–Lu) series. Inset: The crystal structure of $R_4Be_{33}Pt_{16}$ projected along [111] and represented as an arrangement of interpenetrating coordination polyhedrons around R and Pt1 atoms.

samples of $R_4Be_{33}Pt_{16}$ (R = Y, La–Nd, Sm–Lu) were synthesized by arc melting of R (pieces, Ames Laboratory, >99.9%), Be (sheet, Heraeus, >99.9%), and Pt (foil, Chempur, >99.9%) in the 10:60:30 ratio. In order to ensure homogeneity, all samples were arc melted several times, with final mass losses of at most 2%. Small inclusions of secondary phases were identified by several experimental methods (see below), while temperature treatment, as well as changing the initial composition, did not result in completely single-phase samples. Since the amount of Be is hard to quantify analytically (see below), and given that the evaporation losses of Be are unavoidable, the only way to keep control of the sample composition is to follow a careful weighing protocol. None of the samples exhibited any marked air or moisture sensitivity.

Powder x-ray diffraction was performed on a Huber G670 Image plate Guinier camera with a Ge monochromator (Cu $K\alpha_1$, $\lambda = 1.54056$ Å). Phase identification was done using the WinXPow software [32]. The lattice parameters were determined by a least-squares refinement using the peak positions, extracted by profile fitting (WinCSD software [33]). Results are provided in Fig. 1 and Table III. Neighboring phase(s) were found to be present in all samples as impurities (see Table S1 and Figs. S1 and S2 of the Supplemental Material [30]), with the amounts ranging from $<0.41 \pm 0.12$ wt % (R = Gd) to 8.45 ± 0.65 wt % (R = La). Given significantly different properties of the impurity phases, it was possible to determine intrinsic properties of the $R_4Be_{33}Pt_{16}$ compounds.

Chemical composition was studied on polished samples using energy-dispersive x-ray spectroscopy with a Jeol JSM 6610 scanning electron microscope equipped with an UltraDry EDS detector (ThermoFisher NSS7). The semiquantitative analysis was performed with 25 keV acceleration voltage and ≈3 nA beam current. Small inclusions of secondary phases are also visible from backscatter scanning electron micrographs, presented in Figs. S3 and S4 of the Supplemental Material [30]. A quantitative analysis is provided in Table S1 of the Supplemental Material [30]. However, it has to be emphasized that the Be content cannot be reliably analyzed by this method.

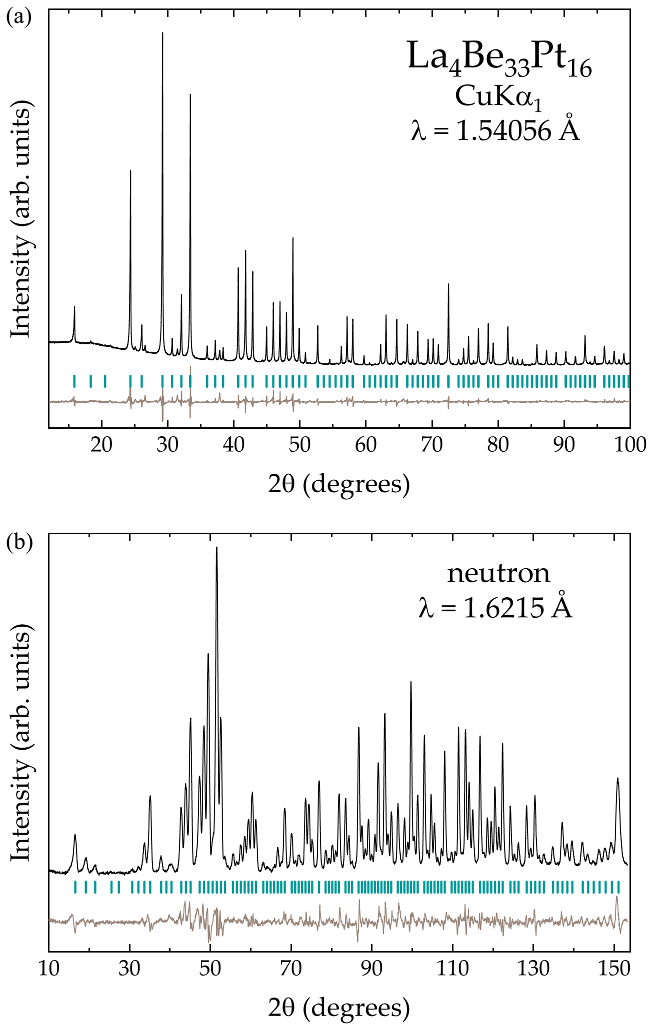

FIG. 2. (a) X-ray and (b) neutron powder diffraction patterns for $La_4Be_{33}Pt_{16}$. Experimental patterns are shown as black solid lines. The blue bars below the patterns correspond to calculated positions of the reflections. The difference curve (beige) indicates a good agreement between theoretical and experimental patterns.

Neutron powder diffraction of $La_4Be_{33}Pt_{16}$ was performed on the ECHIDNA high-resolution diffractometer at the OPAL reactor (ANSTO, Lucas Heights, Australia). The powdered sample was placed in a cylindrical vanadium holder and diffraction data were collected in transmission geometry ($\lambda = 1.6215(1)$ Å). These data, as well as corresponding x-ray diffraction pattern, were used for joint refinement of the crystal structure by the Rietveld method (see Fig. 2 and Tables I and II) [34].

Field-dependent magnetization and temperature-dependent dc-susceptibility measurements were carried out in a Quantum Design (QD) Magnetic Property Measurement System for temperatures between 1.8 and 300 K, and for applied magnetic fields up to $\mu_0 H = 7$ T. The inverse magnetic susceptibility data were fit to the Curie-Weiss law in the temperature region between T = 150 K and T = 300 K, after a temperature-independent contribution M_0 has been subtracted (see Table III for M_0 values). For R = Nd, Ho, Er, and Tm, the magnitude of the Weiss temperature θ_W is rather small, with the sign being highly dependent upon the region of fitting (see

TABLE I. Crystallographic data for $La_4Be_{33}Pt_{16}$ ($Y_4Be_{33}Pt_{16}$ structure type).

Crystal system	Cubic
Space group	$I\bar{4}3d$ (No. 220)
Pearson symbol	$cI212$
Formula units per cell	$Z = 4$
Molar mass	3974.36 g mol^{-1}
Unit cell parameter, a	13.6682(4) Å[a]
Unit cell volume, V	2553.5(2) Å^3
Calculated density	10.33 g cm^{-3}
Parameters refined	52
Neutron diffraction	
Radiation type, λ	Neutron, 1.6215(1) Å
Diffractometer	ECHIDNA at ANSTO (Australia)
Geometry	Transmission
$2\theta_{\min}$, $2\theta_{\max}$, 2θ-step	10.0°, 153.4°, 0.05°
R_B, R_p, R_{wp}	0.049, 0.062, 0.083
X-ray diffraction	
Radiation type, λ	Cu $K\alpha_1$, 1.54056 Å
Diffractometer	Image Plate Guinier camera Huber 670
Geometry	Transmission
$2\theta_{\min}$, $2\theta_{\max}$, 2θ step	12.0°, 100.3°, 0.005°
R_B, R_p, R_{wp}	0.059, 0.122, 0.143

[a] Obtained from powder x-ray diffraction data.

Table II for an estimate of error bars). Therefore, a definitive assessment of coupling mechanisms in these systems is left to a future study. The magnetic hysteresis measurements were taken at the lowest accessible temperature, $T = 1.8$ K. For clarity, the virgin curve has been removed and only the upper quadrant is shown [see, for example, inset of Fig. 8(a) and inset of Fig. 9(a)]. Heat capacity was measured from $T = 0.4$ to 10 K, in magnetic fields up to $\mu_0 H = 9$ T using a QD Physical Property Measurement System. Similar to the other Be-containing material Be_5Pt [35], the electrical resistivity of $R_4Be_{33}Pt_{16}$ (R = Y, La–Nd, Sm–Lu) samples is dominated by that of the secondary phase(s). Therefore, it was not possible to conclusively establish transport properties of $R_4Be_{33}Pt_{16}$ (R = Y, La–Nd, Sm–Lu) compounds. Given nonzero density of states at the Fermi level for R = La, Lu, and Sc systems (see Fig. 5), all compounds of the series are likely metals.

Electronic structure calculations were performed by using the all-electron, full-potential local orbital (FPLO) method [36]. All main results were obtained within the local density approximation (LDA) to the density functional theory (DFT) through the Perdew-Wang parametrization for the exchange-correlation effects [37]. Application of the generalized gradient approximation (GGA) did not reveal essential differences in the electronic structure below and in the vicinity of the Fermi level.

TABLE II. Atomic coordinates, Wyckoff sites, and isotropic displacement parameters (Å^2) for $La_4Be_{33}Pt_{16}$, obtained by joined x-ray-neutron refinement.

Atom	Site	x/a	y/b	z/c	U_{iso}
La1	16c	0.8087(3)	x	x	0.43(9)
Pt1	16c	0.9347(2)	x	x	0.42(7)
Pt2	48e	0.4912(2)	0.8974(3)	0.7763(2)	0.42(5)
Be1	12a	5/8	0	3/4	0.45(12)
Be2	24d	0.9117(4)	0	3/4	0.68(9)
Be3	48e	0.0578(3)	0.9906(3)	0.6663(3)	0.72(6)
Be4	48e	0.6219(3)	0.9165(3)	0.8957(3)	0.73(7)

III. CRYSTAL STRUCTURE

The cubic lattice parameter a of the $R_4Be_{33}Pt_{16}$ compounds follows the trend of the ionic radii for R^{3+} ions, i.e., lanthanide contraction, as depicted in Fig. 1. The clear exception is $Ce_4Be_{33}Pt_{16}$, with significant volume contraction with respect to the isotypic compounds of trivalent R. This indicates that the electronic configuration of Ce in $Ce_4Be_{33}Pt_{16}$ likely deviates from the $4f^1$ value [38]. The lattice parameter of $Yb_4Be_{33}Pt_{16}$ differs only slightly from the monotonic trend (Fig. 1), probably pointing towards possible complexity in its electronic state. Also noticeable is the fact that the unit cell parameter of the $Eu_4Be_{33}Pt_{16}$ compound fits well into the trend for trivalent rare-earth metals, likely indicative of its convoluted ground-state properties [39–51].

The crystal structure was first established for $Y_4Be_{33}Pt_{16}$ by means of x-ray single-crystal data, which is reported in a separate paper [29]. Here we represent the structure of $La_4Be_{33}Pt_{16}$ as a result of the combined refinement using x-ray and neutron powder diffraction data. The latter were necessary to ensure the reliable coordinates of the beryllium atoms (Tables SI and SII, and Fig. S2 [30]). The structure of $La_4Be_{33}Pt_{16}$ is described with one La, four Be, and two Pt crystallographic positions in the noncentrosymmetric space group $I\bar{4}3d$. The coordination environment of the La atom includes 12 Be and 8 Pt species, located at 3.079(2)–3.195(4) Å and 2.912(2)–3.123(2) Å, respectively. Adjacent polyhedra around La atoms are interpenetrating via the Pt1 position and form rodlike arrangements along [111] directions (the trigonal axes of the cubic unit cell, Fig. 1 inset). The voids around (3/8 0 1/4) (Wyckoff site 12a) and at (7/8 0 1/4) (Wyckoff site 12b) have a shape of a bidisphenoid and arise where four polyhedra from different rods meet. While the former are occupied by Be1 atoms, the latter remain empty. The homonuclear Pt-Pt contacts of 2.908(2) Å and 2.937(2) Å are slightly longer than interatomic distances of 2.774 Å, observed in elemental platinum [52]. The interatomic distances Be-Be and Be-Pt cover rather larger intervals of 2.210(4)–2.514(4) Å and 2.335(1)–2.698(2) Å, respectively, indicating a complex bonding scenario in $La_4Be_{33}Pt_{16}$. More detailed analysis of the chemical bonding was performed for aristotype structure of $Y_4Be_{33}Pt_{16}$, revealing a multicenter interaction within the Be-Pt framework [29].

Crystallographic data for $La_4Be_{33}Pt_{16}$ are summarized in Tables I and II. The x-ray powder diffraction and neutron powder diffraction data are shown in Fig. 2.

The powder x-ray diffraction patterns for $R_4Be_{33}Pt_{16}$ (R = La–Nd, Sm–Lu) compounds are shown in Figs. S1 and S2 [30]. On the diffraction patterns, the reflections of the minority phases are marked in yellow. The amount of impurity phases is rather small (see Table S1 [30]); it is therefore easier to identify the impurity phases from the energy-dispersive x-ray spectroscopy measurements, shown in Figs. S3 and S4 [30].

TABLE III. Characteristic parameters for the $R_4Be_{33}Pt_{16}$ (R = Y, La–Nd, Sm–Lu) compounds.

R	a (Å)	T^{*}[a] (K)	M_0 (10^{-4}) (emu mol_R^{-1})	θ_W (K)	μ_{eff} ($\mu_B R^{-1}$)	$\mu_{\mathrm{eff}}^{\mathrm{theory}}$[b] ($\mu_B R^{-1}$)	M(1.8 K, 7 T) ($\mu_B R^{-1}$)	$\mu_{\mathrm{sat}}^{\mathrm{theory}}$[b] ($\mu_B R^{-1}$)
Y	13.4849(3)	0.9 ± 0.1						
La	13.6682(4)	2.5 ± 0.2						
Ce	13.5566(6)	13 ± 1				2.54	0.23	2.14
Pr	13.5986(4)	40 ± 3	1.35	−11 ± 5	4.24 ± 0.05	3.58	1.86	3.20
Nd	13.5762(3)	2.0 ± 0.5	1.35	2 ± 5	3.45 ± 0.05	3.62	1.97	3.27
Sm	13.5452(4)	4.5 ± 0.5	1.35			0.85	0.32	0.71
Eu	13.5394(4)	30 ± 2	1.35	−110 ± 5	4.07 ± 0.05		0.29	
Gd	13.5258(3)	14 ± 1	1.35	20 ± 5	8.26 ± 0.05	7.94	7.21	7.00
Tb	13.5048(4)	10 ± 1	1.34	12 ± 5	9.74 ± 0.05	9.72	6.54	9.00
Dy	13.4930(3)	10 ± 1	1.34	13 ± 5	10.51 ± 0.05	10.65	5.57	10.00
Ho	13.4800(4)	2.9 ± 0.1	1.34	4 ± 5	10.46 ± 0.05	10.61	7.23	10.00
Er	13.4672(3)	3.6 ± 0.1	1.33	1 ± 5	9.30 ± 0.05	9.58	7.09	9.00
Tm	13.4514(3)	3.6 ± 0.1	1.33	−1 ± 5	7.97 ± 0.05	7.56	5.07	7.00
Yb	13.4504(6)	0.4 ± 0.01	1.33	−10 ± 5	3.58 ± 0.05	4.54	1.28	4.00
Lu	13.4366(3)	0.7 ± 0.05						

[a] T^{*} is T_c for superconductors and T_{mag} is for magnets.

[b] Calculated for an R^{3+} ion.

The majority of impurities found in the $R_4Be_{33}Pt_{16}$ (R = La–Nd, Sm–Lu) compounds have been previously characterized (see Table S1 [30]). It is therefore possible to separate the physical properties of $R_4Be_{33}Pt_{16}$ (R = La–Nd, Sm–Lu) compounds from those of the impurity phases. For a detailed description, see Sec. SIII of the Supplemental Material [30].

IV. PHYSICAL PROPERTIES

A. Superconducting compounds

Three compounds from the $R_4Be_{33}Pt_{16}$ series exhibit superconductivity: $Y_4Be_{33}Pt_{16}$ [29], $La_4Be_{33}Pt_{16}$, and $Lu_4Be_{33}Pt_{16}$. The first indication of superconductivity in $La_4Be_{33}Pt_{16}$ is given by a sharp diamagnetic transition at T_c = 2.5 K, as presented in Fig. 3(a). The temperature-dependent magnetic susceptibility was corrected for demagnetization effects according to $4\pi\chi_{\mathrm{eff}} = 4\pi\chi/(1 - N_d\chi)$ with the demagnetizing factor for a spherical or cubic sample geometry $N_d = 1/3$ [53,54]. For the $\mu_0 H = 0.5$ mT curve, the Meissner fraction value is close to 100%, indicating bulk superconductivity. For $\mu_0 H > 0.5$ mT, the low-temperature plateau is not visible, due to it being below the minimum accessible temperature of 1.8 K. Generally, the values of the lower critical

TABLE IV. Characteristic parameters for the $R_4Be_{33}Pt_{16}$ (R = Y, La–Nd, Sm–Lu) series of compounds.

R	γ_n (mJ mol_R^{-1} K^{-2})	γ_{theory}[a] (mJ mol_R^{-1} K^{-2})	γ_{res}[b] (mJ mol_R^{-1} K^{-2})	β[c] (mJ mol_R^{-1} K^{-3})	θ_D (K)	$\lambda_{\text{e-p}}$[d]
Y	18 ± 2	15.7	12.7	4.5 ± 0.5	283 ± 5	0.38–0.47
La	21 ± 2	19.0	2.95	2.3 ± 0.5	355 ± 5	0.37–0.45
Ce	100 ± 2			1.0 ± 0.5	468 ± 5	
Pr	49 ± 2			1.4 ± 0.5	419 ± 5	
Nd						
Sm						
Eu						
Gd						
Tb						
Dy						
Ho						
Er						
Tm						
Yb	40 ± 2			1.1 ± 0.5	454 ± 10	
Lu	21 ± 2	11.7	26.3	2.8 ± 0.5	333 ± 10	0.32–0.40

[a] Calculated based on the density of states at the Fermi level.

[b] γ_{res} was determined as C_e/T at the lowest temperature $T = 0.35$ K and in $H = 0$. Note that given low superconducting temperature of the R = Y and R = Lu compounds, the values of γ_{res} are likely overestimated.

[c] It is possible that the difference found in the values of β for isostructural $R_4Be_{33}Pt_{16}$ compounds arises due to the presence of impurities that affect the fit of the specific heat data.

[d] Calculated using Eq. (1).

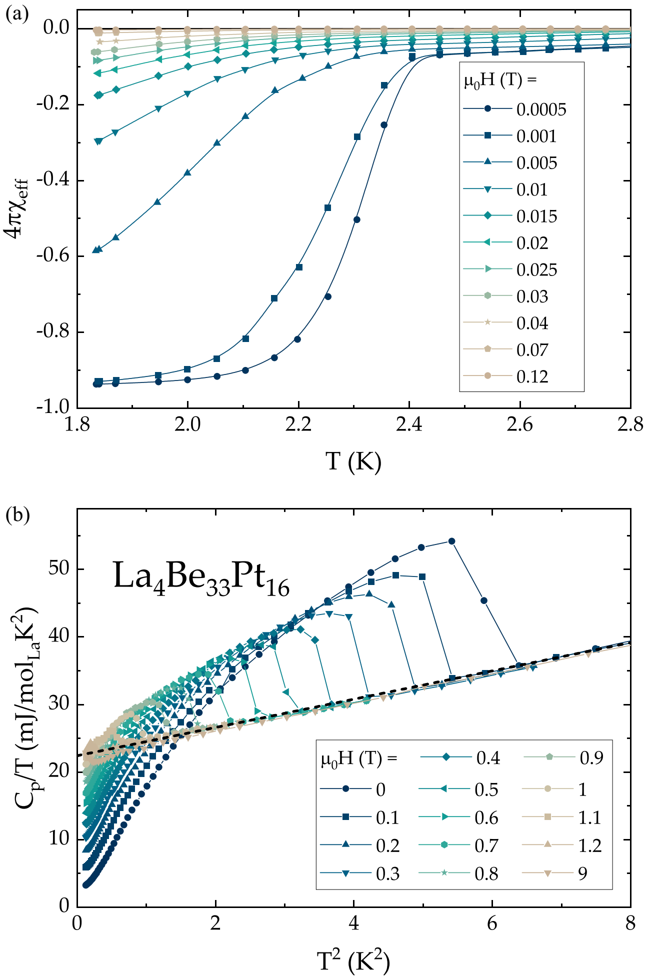

FIG. 3. (a) Zero-field-cooled temperature-dependent magnetic susceptibility data for $La_4Be_{33}Pt_{16}$, scaled by 4π and corrected for the demagnetization effects, in $0.0005 \leqslant \mu_0 H \leqslant 0.12$ T. (b) Specific heat data, scaled by temperature T, as a function of T^2 in $0 \leqslant \mu_0 H \leqslant 9$ T. The dashed line represents a fit from which the value of γ_n was extracted.

field H_{c1} are defined as the field at which the $M(H)$ curves deviate from the line with the initial slope of the $M(H)$ curve. However, in this case, the lowest experimentally accessible temperature was not sufficient to allow for such an analysis.

The specific heat data of $La_4Be_{33}Pt_{16}$, shown in Fig. 3(b), also confirm bulk superconductivity. A linear fit to C_p/T vs T^2 (dashed line) gives the value of the Sommerfeld coefficient $\gamma_n = 21$ mJ mol_R^{-1} K^{-2}. From the Debye temperature, the strength of the electron-phonon coupling is estimated using the McMillan equation [55]:

$$\lambda_{\text{e-p}} = \frac{1.04 + \mu^* \ln\left(\frac{\theta_D}{1.45T_c}\right)}{(1 - 0.62\mu^*)\ln\left(\frac{\theta_D}{1.45T_c}\right) - 1.04}. \tag{1}$$

The value of $0.37 \leqslant \lambda_{\text{e-p}} \leqslant 0.45$ is indicative of weak-coupling superconductivity. The value for the jump in the electronic specific heat $\Delta C_e/\gamma_n T_c \approx 1.95$ is slightly larger than the Bardeen-Cooper-Schrieffer (BCS) value ($\Delta C_e/\gamma_n T_c = 1.43$). The residual electronic specific heat coefficient $\gamma_{\text{res}} = 2.95\ \text{mJ}\ \text{mol}_R^{-1}\ \text{K}^{-2}$ was estimated as $\gamma_{\text{res}} = C_e/T$ at the lowest temperature $T = 0.35$ K and in $H = 0$. In a conventional superconductor, like in our case, γ_{res} is due to metallic impurity phases. Thus the superconductivity of $La_4Be_{33}Pt_{16}$ is a bulk effect, consistent with the full Meissner fraction, observed in magnetization data [Fig. 3(a)].

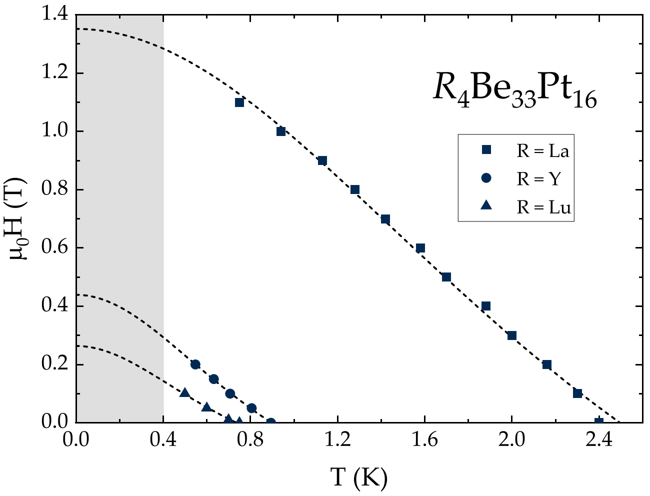

FIG. 4. The H-T phase diagram for $La_4Be_{33}Pt_{16}$ (squares), $Y_4Be_{33}Pt_{16}$ (circles), and $Lu_4Be_{33}Pt_{16}$ (triangles) with the values of $H_{c2}(T)$ taken from the specific heat data. Dashed lines are Ginzburg-Landau [Eq. (2)] fits to the data, and the shaded region represents temperatures, inaccessible in the current work.

The $Y_4Be_{33}Pt_{16}$ and $Lu_4Be_{33}Pt_{16}$ compounds enter the superconducting state below $T_c = 0.9$ K and $T_c = 0.7$ K, respectively. Their modest values of γ_n (see Table IV) indicate a nearly negligible effective mass enhancement. From the equal entropy construct (not shown), the ratios $\Delta C_e/\gamma_n T_c \approx 1.80$ ($R = \text{Y}$) and $\Delta C_e/\gamma_n T_c \approx 1.64$ ($R = \text{Lu}$) are somewhat higher than the BCS value. The Debye temperatures θ_D, as well as the value of the electron-phonon coupling $\lambda_{\text{e-p}}$, are comparable to

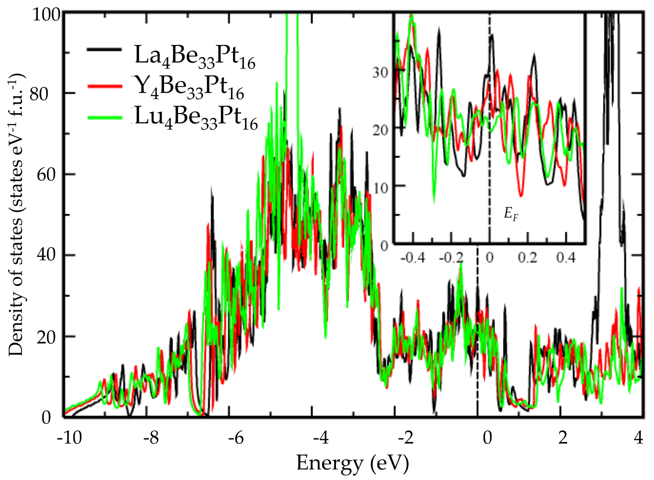

FIG. 5. Total electronic density of states for $R_4Be_{33}Pt_{16}$ [$R = \text{La}$ (black), Y (red), and Lu (green)]. The large peaks at around 3 and −4.5 eV originate from unoccupied La 4f and fully occupied Lu 4f states, respectively. The inset shows an enlarged view around the Fermi level E_F.

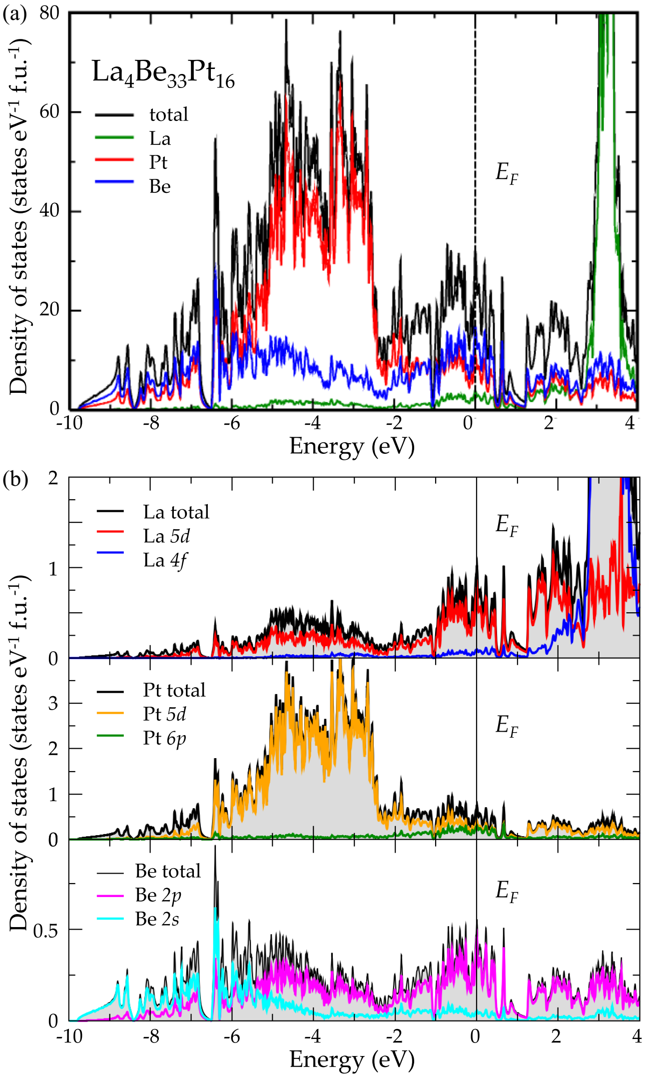

FIG. 6. (a) Total density of states (blue) together with the contributions due to La (green), Be (blue), and Pt (red) atoms in $La_4Be_{33}Pt_{16}$. The contributions for the two different Pt sites are rather similar and are therefore combined. The same applies for the four different Be sites. The large peak at around 3 eV is due to the unoccupied La $4f$ states. (b) Orbital-resolved atomic density of states for the main contributions to the valence band. As in the upper panel, the similar contributions for the crystallographically different Pt and Be sites are combined. Note that for better presentation the scales are different.

those of $La_4Be_{33}Pt_{16}$ (see Table IV). As expected for type-II superconductors, the application of magnetic field results in a gradual suppression of the critical temperature T_c. The evolution of the upper critical field H_{c2} as a function of temperature is fit using the Ginzburg-Landau relation [56]:

$$H_{c2}(T) = H_{c2}(0)\frac{1-\left(\frac{T}{T_c}\right)^2}{1+\left(\frac{T}{T_c}\right)^2}. \qquad (2)$$

In Fig. 4, the Ginzburg-Landau fit is represented by a dashed line for $La_4Be_{33}Pt_{16}$ (squares), $Y_4Be_{33}Pt_{16}$ (circles), and $Lu_4Be_{33}Pt_{16}$ (triangles).

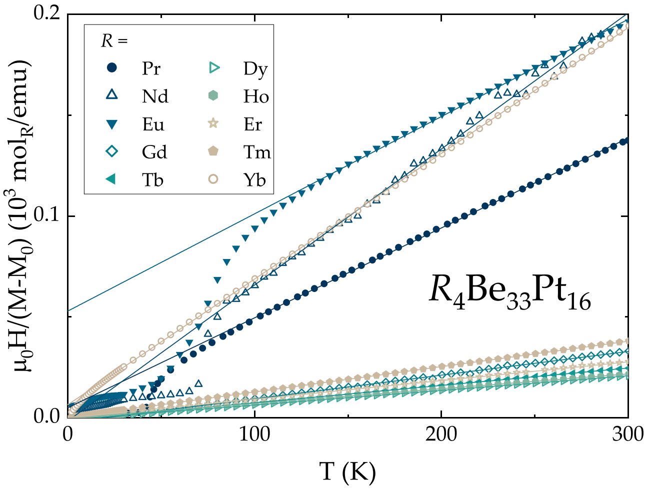

FIG. 7. Temperature-dependent inverse magnetic susceptibility $\chi = (M - M_0)/H$ for $R_4Be_{33}Pt_{16}$ (R = Pr, Nd, Eu–Yb). The solid lines represent fits to the Curie-Weiss law (see Secs. II and IV B for details, as well as Table III for the summary of μ_{eff} and θ_W values.

The electronic structure of $R_4Be_{33}Pt_{16}$ (R = Y, La, and Lu) compounds was examined by means of DFT calculations. The choice of the exchange correlation potential—LDA vs GGA—did not yield a significant difference in the electronic structure (see Fig. S7 [30]). In order to evaluate the sensitivity of the calculations to atomic coordinates, they were optimized with respect to the total energy for all three compounds using the experimental atomic positions of the La compound as starting values. The optimized atomic positions for R = La are within error bars of the experimental ones, listed in Table SII [30]. The optimized atomic positions for R = Y and R = Lu are provided in Tables S2 and S3 [30]. Nonetheless, changes of the atomic positions within the experimental error bars have a negligible influence on the resulting electronic structure.

On a larger energy scale, the valence band of the three systems looks very similar, as evident from Fig. 5. As one may expect, the band width scales inversely with the lattice parameter. Due to the increasing overlap with decreasing inter-atomic distance, the R = Lu compound has a slightly larger band width than the R = Y compound, whereas the R = La system has the smallest valence band width. Although the total valence bands are similar, the region near the Fermi level E_F shows pronounced differences, as can be seen in the inset of Fig. 5. Comparing the calculated $N(E_F)$ with that extracted from the Sommerfeld coefficient, a rather small mass renormalization is obtained: ~1.1 for the R = La (γ_{theory} = 19.0 mJ mol_R^{-1} K^{-2}) and R = Y (γ_{theory} = 15.7 mJ mol_R^{-1} K^{-2}), and ~1.8 for the R = Lu system (γ_{theory} = 11.7 mJ mol_R^{-1} K^{-2}). The reason for this pronounced difference in mass renormalization for these ostensibly similar materials remains unclear.

The partial contributions of the atomic states are very similar for all three compounds, as shown in Fig. 6 for $La_4Be_{33}Pt_{16}$. The low-lying states (below about −8 eV) originate predominantly from Be 2*s* states. Between about −6.5 and −2.5 eV, an essentially fully filled Pt 3*d* state is found.

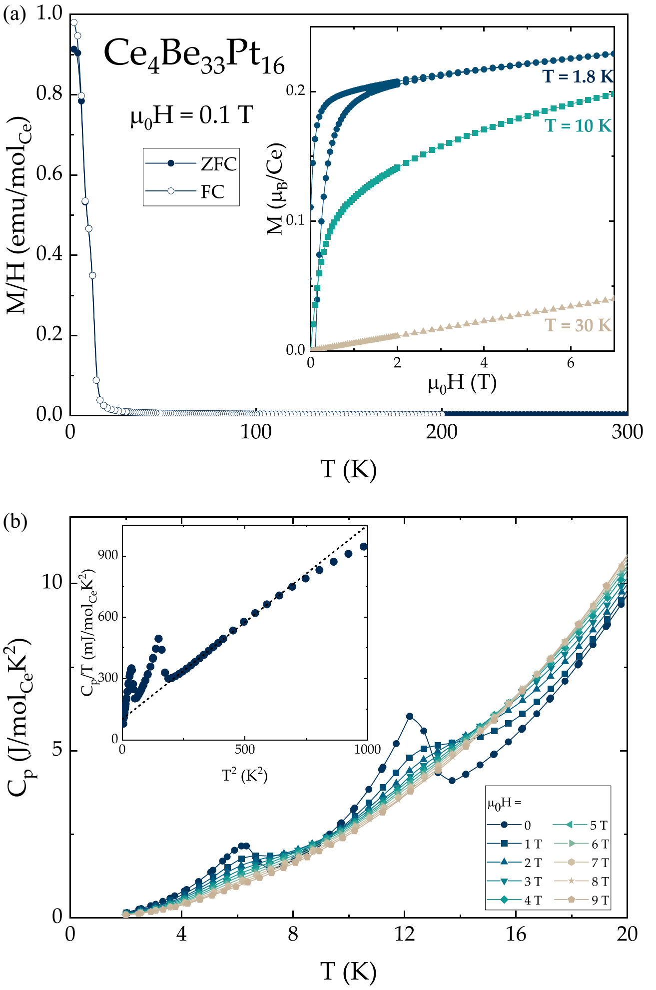

FIG. 8. (a) Temperature-dependent magnetic susceptibility for $Ce_4Be_{33}Pt_{16}$ in an applied magnetic field $\mu_0 H = 0.1$ T. Inset: An upper quadrant of the $T = 1.8$ K hysteresis loop (with the virgin curve removed), together with magnetic isotherms, measured at $T = 10$ and 30 K. (b) Specific heat as a function of temperature in $0 \leqslant \mu_0 H \leqslant 9$ T. Inset: C_p/T vs T^2 in $H = 0$, along with a linear fit (dashed line).

Around the Fermi level, the dominating states originate from La 5*d* and Pt 5*d* electrons and from Be 2*p* states. Taking into account the number of atoms per formula unit, the contribution of the different individual atoms (per site) is of the same order. The inclusion of spin-orbit coupling (see Fig. S8 [30]) has no significant influence on the valence states, resulting in a small decrease of $N(E_F)$ for all three compounds.

It is rather likely that $Y_4Be_{33}Pt_{16}$, $La_4Be_{33}Pt_{16}$, and $Lu_4Be_{33}Pt_{16}$ superconductors are conventional, given modest values of the electron-phonon and spin-orbit coupling. Further analysis of superconducting properties of $La_4Be_{33}Pt_{16}$, $Y_4Be_{33}Pt_{16}$, and $Lu_4Be_{33}Pt_{16}$ compounds by means of muon spin rotation, relaxation, and resonance (μSR) would be of interest [57–61]. The μSR experiments will allow to establish whether $La_4Be_{33}Pt_{16}$, $Y_4Be_{33}Pt_{16}$, and $Lu_4Be_{33}Pt_{16}$ are definitively type-II or type-I superconductors [62–65], as well as help pinpoint their superconducting pairing mechanism.

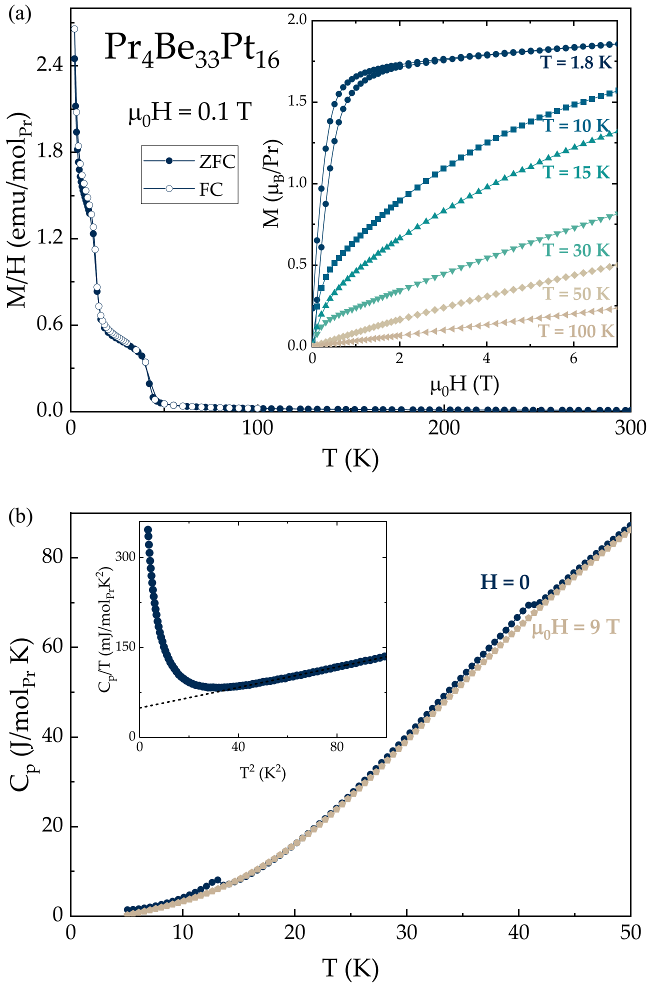

FIG. 9. (a) Temperature-dependent magnetic susceptibility for $Pr_4Be_{33}Pt_{16}$ in $\mu_0 H = 0.1$ T. Inset: An upper quadrant of the $T = 1.8$ K hysteresis loop with the virgin curve removed, together with the field-dependent magnetization data, taken at various temperatures. (b) Specific heat in $\mu_0 H = 0$ (blue) and $\mu_0 H = 9$ T (beige). Inset: C_p/T vs T^2 in $\mu_0 H = 0$, along with a linear fit (dashed line).

B. Magnetic compounds

Due to synthesis complications brought on by specificity of Be (see Sec. II), the majority of the specimens of the nonsuperconducting $R_4Be_{33}Pt_{16}$ compounds suffer from significant inclusions of the secondary phases, some of which are ferro- or antiferromagnetic. For a quantitative description of observed impurity phases see Table S1 [30]. While several synthesis attempts did not result in an appreciable sample quality improvement, the physical properties of $R_4Be_{33}Pt_{16}$ compounds have been decoupled from those of the respective impurity phases. Nonetheless, the current work is a preliminary report on a new family of materials that are certainly worthy of consequent in-depth investigations.

The majority of the $R_4Be_{33}Pt_{16}$ compounds order magnetically. The inverse magnetic susceptibility, after the temperature-independent contribution M_0 (see Table III) has been subtracted, is shown in Fig. 7. Most of the compounds follow a Curie-Weiss law, as evident from the linear fits (solid lines). The values of the effective magnetic moment μ_{eff} and the Weiss temperature θ_W extracted from the fits are summarized in Table III. These values are similar to those expected for a R^{3+} ion $\mu_{\text{eff}}^{\text{theory}}$, except for R = Eu, which is probably indicative of a complex electronic state of this compound. The Weiss temperature θ_W for R = Gd, Tb, and Dy has positive values and is comparable to the magnitude of the ordering temperature T_{mag}, which is likely indicative of predominantly ferromagnetic coupling in these systems. The negative values of the Weiss temperature θ_W for R = Pr, Eu, and Yb are likely indicative of antiferromagnetic coupling in these materials. A significant difference between the ordering and the Weiss temperatures for R = Pr, Eu, and Yb, coupled with bifurcation of zero-field-cooled and field-cooled magnetic susceptibility data (Figs. 9(a) and S11 [30]) signal possible crystallographic frustration. A possible scenario of crystallographic frustration is depicted in Fig. S5 [30]. For R = Nd, Ho, Er, and Tm, the magnitude of the Weiss temperature θ_W is rather small, with the sign being dependent upon the region of fitting. Therefore, in order to fully understand the magnetism of $R_4Be_{33}Pt_{16}$ (R = Ce–Nd, Sm–Yb) materials, more in-depth studies are needed.

Below, a brief description of magnetic properties of the $Ce_4Be_{33}Pt_{16}$, $Pr_4Be_{33}Pt_{16}$, and $Yb_4Be_{33}Pt_{16}$ compounds is presented, with the remaining compounds shown in Section SIII of the Supplemental Material [30].

The $Ce_4Be_{33}Pt_{16}$ sample displays two magnetic transitions, one at T = 6 K and another at T = 13 K. Features, associated with these transitions, can be seen in temperature-dependent magnetization [Fig. 8(a)] and specific heat [Fig. 8(b)]. The origin of the T = 6 K can be ascribed to the CePt impurity, which orders ferromagnetically at T_C = 5.8 K [66]. While the amount of the CePt impurity is rather small (∼0.4 wt %; see Table S1 [30]), its presence can be clearly identified in Figs. S1(b) and S3(b) [30]. It was not yet possible to eliminate the CePt impurity (see Sec. II).

The $Ce_4Be_{33}Pt_{16}$ compound orders magnetically below T = 13 K. Upon application of a magnetic field, the size of the feature is gradually diminished, while its position moves up in temperature [see Fig. 8(b)]. This suggests ferromagnetic character of the T = 13 K transition. Predominantly ferromagnetic coupling is also indicated by the shape of magnetic isotherms, as well as the bifurcation of the zero-field-cooled (solid symbols) and field-cooled (open symbols) data, shown in Fig. 8(a). The magnitude of M(1.8 K, 7 T) is considerably smaller than the theoretical one (see Table III), which can perhaps be explained by the valence of Ce being somewhere between 3+ and 4+. This is also consistent with the significant volume contraction of $Ce_4Be_{33}Pt_{16}$, compared to the trivalent isotypic compounds (see Sec. III and Fig. 1). The value of the Sommerfeld coefficient γ_n = 100 mJ mol_R^{-1} K^{-2} [inset of Fig. 8(b)] is moderate.

The $Pr_4Be_{33}Pt_{16}$ sample shows two consecutive magnetic transitions, one at T = 40 K and another at T = 14 K, as can be seen from Fig. 9(a). The lower transition is associated with the PrPt phase, which orders ferromagnetically below T_C = 15 K [67]. The amount of the PrPt impurity is rather small (∼1.1 wt %, see Table S1 [30]); however, its presence can be seen in x-ray powder patterns and backscatter electron micrographs, Figs. S1(c) and S3(c) [30]. Similarly to the case of $Ce_4Be_{33}Pt_{16}$, it was not possible to eliminate this impurity from our samples by preparation.

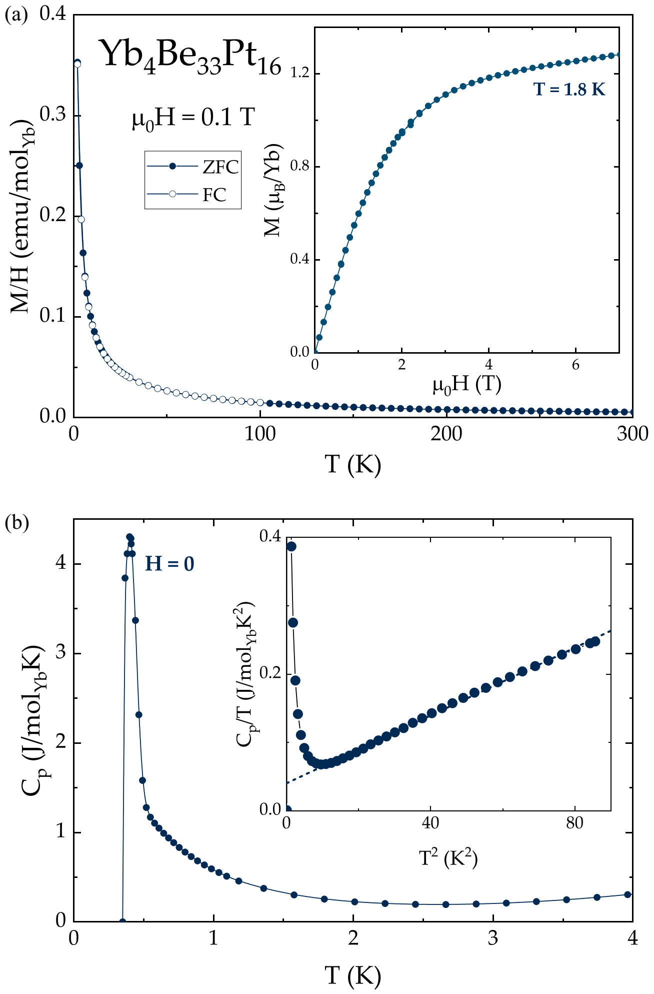

FIG. 10. (a) Temperature-dependent magnetic susceptibility for $Yb_4Be_{33}Pt_{16}$ in μ_0H = 0.1 T. Inset: An upper quadrant of the T = 1.8 K hysteresis loop, with the virgin curve removed for clarity. (b) Specific heat of $Yb_4Be_{33}Pt_{16}$, scaled by temperature T, C_p/T as a function of T^2 in μ_0H = 0. The dashed line represents a fit from which the value of γ_n was extracted.

The $Pr_4Be_{33}Pt_{16}$ compound orders magnetically below T = 40 K. Upon application of magnetic field, the feature corresponding to the magnetic transition disappears [Fig. 9(b)]. This, together with negative value of the Weiss temperature θ_W (Table III), overlapping zero-field-cooled (solid symbols) and field-cooled (open symbols) magnetic susceptibility data [Fig. 9(a)], as well as the shape of the magnetic isotherms [inset of Fig. 9(a)], are likely indicative of mostly antiferromagnetic coupling in $Pr_4Be_{33}Pt_{16}$. However, the definitive coupling mechanism can possibly be established via neutron-scattering experiments, which are currently under way. The value of the effective magnetic moment μ_{eff} = 4.24 μ_B/Pr is larger than the expected one ($\mu_{\text{eff}}^{\text{theory}}$ = 3.58 μ_B/Pr). The low-temperature specific heat of $Pr_4Be_{33}Pt_{16}$ displays an upturn, which can likely arise from a Schottky anomaly. Nonetheless, at higher temperatures, linear C_p/T vs T^2 behavior is recovered, yielding γ_n = 50 mJ mol_R^{-1} K^{-2}.

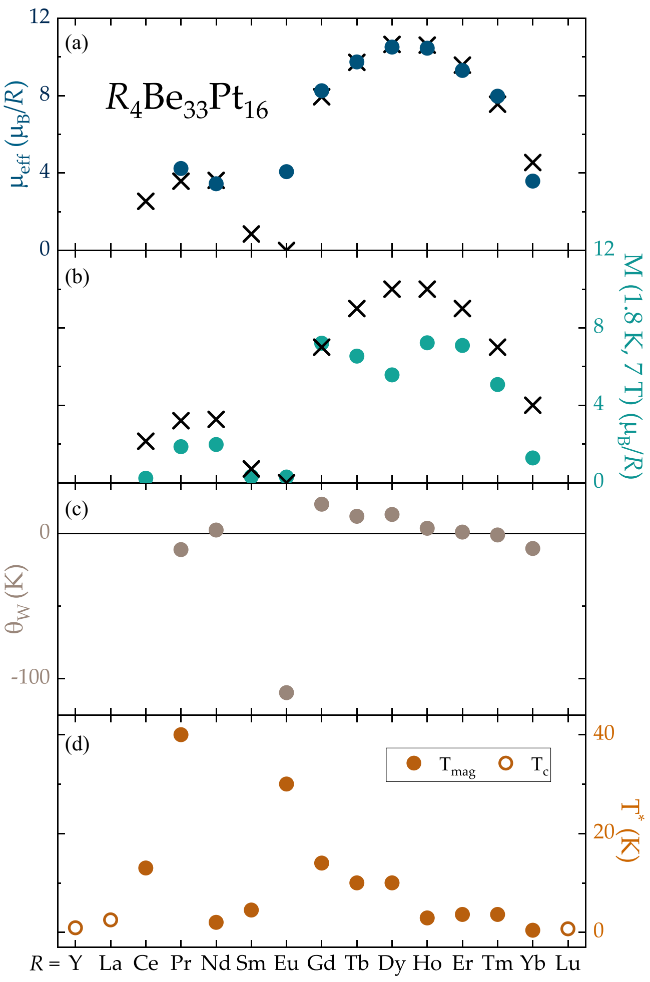

FIG. 11. Magnetic parameters for the $R_4Be_{33}Pt_{16}$ series vs R: (a) the effective magnetic moment μ_{eff} (points) along with its expected value (crosses), (b) $M(1.8\,\text{K}, 7\,\text{T})$ (points) along with its expected value (crosses), (c) the Weiss temperature θ_{W}, and (d) the characteristic ordering temperature T^*—magnetic ordering temperature T_{mag} (solid symbols) or superconducting transition temperature T_{c} (open symbols).

The magnetic and specific heat data for $Yb_4Be_{33}Pt_{16}$ are shown in Fig. 10. A transition, observed at $T = 0.4$ K, is likely of antiferromagnetic character, given the negative value of the Weiss temperature θ_{W} (see Table III). At higher temperatures, a linear fit to the C_p/T vs T^2 data [dashed line, inset of Fig. 10(b)] yields $\gamma_n = 22$ mJ $\text{mol}_R^{-1}\,\text{K}^{-2}$. Similar to the other members of the $R_4Be_{33}Pt_{16}$ series, the effective mass enhancement in $Yb_4Be_{33}Pt_{16}$ is nearly negligible.

V. CONCLUSIONS

In this work, we present an initial theoretical and experimental study of a series of 15 rare-earth-based $R_4Be_{33}Pt_{16}$ compounds with R = Y, La–Nd, Sm–Lu, crystallizing in the noncentrosymmetric space group $I\bar{4}3d$.

Three compounds (R = Y, La, and Lu) exhibit bulk superconductivity below $T_c = 0.9$, 2.5, and 0.7 K, respectively. All three systems are likely type-II, weakly coupled BCS-like superconductors, extending the family of very few known Pt-based superconducting materials [68]. It appears, that both electron-phonon and spin-orbit coupling strengths are rather weak, which could be indicative of a conventional superconducting pairing mechanism. The values of the density of states at the Fermi level are proportional to the values of the superconducting temperature T_c.

The rest of the $R_4Be_{33}Pt_{16}$ compounds show magnetic ordering, with ordering temperatures ranging from $T_{\text{mag}} = 0.4$ K (R = Yb) to $T_{\text{mag}} = 40$ K (R = Pr). Several members of the series (R = Pr, Eu, and Yb) exhibit signs of glassy behavior. The R = Eu and R = Ce compounds most likely display quite complex electronic state. Overall, the ground states of the $R_4Be_{33}Pt_{16}$ (R = Y, La–Nd, Sm–Lu) compounds vary strongly, as summarized in Fig. 11.

The newly discovered $R_4Be_{33}Pt_{16}$ (R = Y, La–Nd, Sm–Lu) materials expand the understanding of crystal chemistry of solid-state materials, while simultaneously giving an insight on which parameters impact the physical properties of a given system.

ACKNOWLEDGMENTS

We are thankful to W. Schnelle for fruitful discussions, H. Borrmann and S. Hückmann for assistance in powder diffraction experiments, K. Vanatko and R. Gellrich for help with the preparative work, as well as U. Nitsche for technical support. E.S. is grateful for the support of the Christiane Nüsslein-Volhard-Stiftung.

[1] R. Gumeniuk, A. N. Yaresko, W. Schnelle, M. Nicklas, K. O. Kvashnina, C. Hennig, Y. Grin, and A. Leithe-Jasper, Phys. Rev. B **97**, 174405 (2018).

[2] R. Gumeniuk, in *Handbook on the Physics and Chemistry of Rare Earths* (Elsevier/North Holland Publishing Company, Amsterdam, 2018), Vol. 54, p. 43.

[3] G. J. Snyder and E. S. Toberer, Nat. Mater. **7**, 105 (2008).

[4] M. B. Gamza, R. Gumeniuk, U. Burkhardt, W. Schnelle, H. Rosner, A. Leithe-Jasper, and A. Ślebarski, Phys. Rev. B **95**, 165142 (2017).

[5] Q. Zheng, R. Gumeniuk, W. Schnelle, Y. Prots, U. Burkhardt, and A. Leithe-Jasper, Solid State Sci. **55**, 93 (2016).

[6] Q. Zheng, R. Gumeniuk, H. Borrmann, W. Schnelle, A. A. Tsirlin, H. Rosner, U. Burkhardt, M. Reissner, Y. Grin, and A. Leithe-Jasper, Dalton Trans. **45**, 9590 (2016).

[7] M. G. Kanatzidis, R. Pöttgen, and W. Jeitschko, Angewandte Chemie International Edition **44**, 6996 (2005).

[8] W. A. Phelan, M. C. Menard, M. J. Kangas, G. T. McCandless, B. L. Drake, and J. Y. Chan, Chem. Mater. **24**, 409 (2012).

[9] R. Gumeniuk, H. Borrmann, A. Ormeci, H. Rosner, W. Schnelle, M. Nicklas, Y. Grin, and A. Leithe-Jasper, Z. Kristallogr. Cryst. Mater. **225**, 531 (2010).

[10] A. K. Pathak, D. Paudyal, Y. Mudryk, and V. K. Pecharsky, Phys. Rev. B **96**, 064412 (2017).

[11] E. Svanidze, A. Amon, R. Borth, Y. Prots, M. Schmidt, M. Nicklas, A. Leithe-Jasper, and Y. Grin, Phys. Rev. B **99**, 220403 (2019).

[12] M. Feig, M. Bobnar, I. Veremchuk, C. Hennig, U. Burkhardt, R. Starke, B. Kundys, A. Leithe-Jasper, and R. Gumeniuk, J. Phys.: Condens. Matter **29**, 495603 (2017).

[13] R. Lemaire and D. Paccard, Bull. Soc. Fr. Mineral. Cristallogr. **92**, 9 (1969).

[14] K. H. Buschow, Rep. Prog. Phys. **40**, 1179 (1977).

[15] K. H. Buschow, Rep. Prog. Phys. **42**, 1373 (1979).

[16] K. H. Buschow, P. C. Bouten, and A. R. Miedema, Rep. Prog. Phys. **45**, 937 (1982).

[17] M. S. Torikachvili, J. W. Chen, Y. Dalichaouch, R. P. Guertin, M. W. McElfresh, C. Rossel, M. B. Maple, and G. P. Meisner, Phys. Rev. B **36**, 8660 (1987).

[18] J. F. Herbst, Rev. Mod. Phys. **63**, 819 (1991).

[19] H. Li and J. M. D. Coey, *Magnetic Properties of Ternary Rare-Earth Transition-Metal Compounds* (Elsevier, Amsterdam, 1991).

[20] J. J. M. Franse and R. J. Radwanski, *Magnetic Properties of Ternary Rare-Earth Transition-Metal Compounds* (Elsevier, Amsterdam, 1993).

[21] P. Quebe, L. J. Terbüchte, and W. Jeitschko, J. Alloys Compd. **302**, 70 (2000).

[22] R. Gumeniuk, M. Schöneich, K. O. Kvashnina, L. Akselrud, A. A. Tsirlin, M. Nicklas, W. Schnelle, O. Janson, Q. Zheng, C. Curfs *et al.*, Dalton Trans. **44**, 5638 (2015).

[23] L. Ke and D. D. Johnson, Phys. Rev. B **94**, 24423 (2016).

[24] J. G. Bunzli and V. K. Pecharsky, in *Handbook on the Physics and Chemistry of Rare Earths* (Elsevier, Amsterdam, 2018).

[25] E. Bauer, G. Hilscher, H. Michor, C. Paul, E. W. Scheidt, A. Gribanov, Y. Seropegin, H. Noël, M. Sigrist, and P. Rogl, Phys. Rev. Lett. **92**, 27003 (2004).

[26] R. J. Cava, B. Batlogg, T. Siegrist, J. J. Krajewski, W. F. Peck, S. Carter, and R. J. Felder, Phys. Rev. B **49**, 12384(R) (1994).

[27] P. L. Paulose, S. K. Dhar, A. D. Chinchure, E. Alleno, C. Godart, L. C. Gupta, and R. Nagarajan, Phys. C **399**, 165 (2003).

[28] P. Alessia, N. Kumar, P. Manfrinetti, and S. K. Dhar, J. Appl. Phys. **109**, 07E134 (2011).

[29] A. Amon, E. Svanidze, Y. Prots, M. Nicklas, U. Burkhardt, A. Ormeci, A. Leithe-Jasper, and Y. Grin, Dalton Trans. **49**, 9362 (2020).

[30] See Supplemental Material at http://link.aps.org/supplemental/10.1103/PhysRevMaterials.5.074801 for additional information on (i) crystallographic information, (ii) neutron and x-ray diffraction, (iii) band structure calculations, and (iv) physical properties of R_4Be$_{33}$Pt$_{16}$ (R = Nd - Tm) compounds.

[31] A. Leithe-Jasper, H. Borrmann, and W. Hönle, Max Planck Institute for Chemical Physics of Solids, Scientific Report, 2006 (unpublished), http://www2.cpfs.mpg.de/web/docs/scientreport/report2006_data/SR%20pages24-27.pdf?cpfs_id=000469.

[32] WinXPow (Version 2.08); STOE and Cie GmbH, Darmstadt, Germany, 2003, https://www.stoe.com/product/software-powder-xrd/.

[33] L. Akselrud and Y. Grin, J. Appl. Crystallogr. **47**, 803 (2014).

[34] J. Rodríguez-Carvajal, Physica B: Condens. **192**, 55 (1993).

[35] A. Amon, E. Svanidze, A. Ormeci, M. König, D. Kasinathan, D. Takegami, Y. Prots, Y. F. Liao, K. D. Tsuei, L. H. Tjeng *et al.*, Angew. Chem. Int. Ed. **58**, 15928 (2019).

[36] K. Koepernik and H. Eschrig, Phys. Rev. B **59**, 1743 (1999).

[37] J. P. Perdew and Y. Wang, Phys. Rev. B **45**, 13244 (1992).

[38] A. Iandelli and A. Palenzona, in *Handbook on the Physics and Chemistry of Rare Earths* (Elsevier/North Holland Publishing Company, Amsterdam, 1979), Vol. 2, p. 48.

[39] E. Morsen, B. D. Mosel, W. Muller-Warmuth, M. Reehuis, and W. Jeitschko, J. Phys. C Solid State Phys. **21**, 3133 (1988).

[40] I. Felner and I. Nowik, J. Phys. Chem. Solids **45**, 419 (1984).

[41] S. Seiro, K. Kummer, D. Vyalikh, N. Caroca-Canales, and C. Geibel, Phys. Status Solidi **250**, 621 (2013).

[42] F. Stegemann, T. Block, S. Klenner, and O. Janka, Chem. Eur. J. **25**, 3505 (2019).

[43] T. Harmening and R. Pöttgen, Z. Naturforsch. **65**, 90 (2010).

[44] I. Felner, Solid State Commun. **21**, 267 (1977).

[45] R. Didchenko and F. P. Gortsema, J. Phys. Chem. Solids **24**, 863 (1963).

[46] B. J. Ruck, H. J. Trodahl, J. H. Richter, J. C. Cezar, F. Wilhelm, A. Rogalev, V. N. Antonov, B. D. Le, and C. Meyer, Phys. Rev. B **83**, 174404 (2011).

[47] E. V. Sampathkumaran, L. C. Gupta, R. Vijayaraghavan, K. V. Gopalakrishnan, R. G. Pillay, and H. G. Devare, J. Phys. C: Solid State Phys. **14**, 237 (1981).

[48] K. A. Gschneidner, J. Less-Common Met. **17**, 13 (1969).

[49] Z. Song, J. Liao, X. Ding, T. Zhou, and Q. L. Liu, J. Lumin. **132**, 1768 (2012).

[50] R. Gumeniuk, W. Schnelle, M. A. Ahmida, M. M. Abd-Elmeguid, K. O. Kvashnina, A. A. Tsirlin, A. Leithe-Jasper, and C. Geibel, J. Phys. Condens. Matter **28**, 115601 (2016).

[51] R. Gumeniuk, M. Schmitt, C. Loison, W. Carrillo-Cabrera, U. Burkhardt, G. Auffermann, M. Schmidt, W. Schnelle, C. Geibel, A. Leithe-Jasper *et al.*, Phys. Rev. B **82**, 235113 (2010).

[52] J. Donohue, *The Structure of Elements* (John Wiley & Sons/New York, Sydney, Toronto, 1974).

[53] J. A. Osborn, Phys. Rev. **67**, 351 (1945).

[54] A. Aharoni, J. Appl. Phys. **83**, 3432 (1998).

[55] W. L. McMillan, Phys. Rev. **167**, 331 (1968).

[56] M. Tinkham, *Introduction to Superconductivity* (McGraw-Hill, New York, 1996).

[57] M. A. Khan, A. B. Karki, T. Samanta, D. Browne, S. Stadler, I. Vekhter, A. Pandey, S. Teknowijoyo, K. Cho, R. Prozorov *et al.*, Phys. Rev. B **94**, 144515 (2016).

[58] R. P. Singh, A. D. Hillier, B. Mazidian, J. Quintanilla, J. F. Annett, D. M. Paul, G. Balakrishnan, and M. R. Lees, Phys. Rev. Lett. **112**, 107002 (2014).

[59] D. Singh, J. A. Barker, A. Thamizhavel, D. M. K. Paul, A. D. Hillier, and R. P. Singh, Phys. Rev. B **96**, 180501(R) (2017).

[60] P. K. Biswas, H. Luetkens, T. Neupert, T. Sturzer, C. Baines, G. Pascua, A. P. Schnyder, M. H. Fischer, J. Goryo, M. R. Lees *et al.*, Phys. Rev. B **87**, 180503(R) (2013).

[61] J. A. T. Barker, D. Singh, A. Thamizhavel, A. D. Hillier, M. R. Lees, G. Balakrishnan, D. M. Paul, and R. P. Singh, Phys. Rev. Lett. **115**, 267001 (2015).

[62] A. Amon, A. Ormeci, M. Bobnar, L. G. Akselrud, M. Avdeev, R. Gumeniuk, U. Burkhardt, Y. Prots, C. Hennig, A. Leithe-Jasper *et al.*, Acc. Chem. Res. **51**, 214 (2018).

[63] J. Beare, M. Nugent, M. N. Wilson, Y. Cai, T. J. Munsie, A. Amon, A. Leithe-Jasper, Z. Gong, S. L. Guo, Z. Guguchia *et al.*, Phys. Rev. B **99**, 134510 (2019).

[64] R. Khasanov, R. Gupta, D. Das, A. Amon, A. Leithe-Jasper, and E. Svanidze, Phys. Rev. Res. **2**, 023142 (2020).

[65] R. Khasanov, R. Gupta, D. Das, A. Leithe-Jasper, and E. Svanidze, Phys. Rev. B **102**, 014514 (2020).

[66] B. J. Holt, J. D. Ramsden, H. H. Sample, and J. G. Huber, Physica C **107**, 255 (1981).

[67] A. Castets, D. Gignoux, J. C. Gomez-Sal, and E. Roudaut, Solid State Commun. **44**, 1329 (1982).

[68] M. Fujioka, M. Ishimaru, T. Shibuya, Y. Kamihara, C. Tabata, H. Amitsuka, A. Miura, M. Tanaka, Y. Takano, H. Kaiju *et al.*, J. Am. Chem. Soc. **138**, 9927 (2016).